Metals and Materials International (2018) 24:840–844
https://doi.org/10.1007/s12540-018-0101-z

Three Distinct Deformation Behaviors of Cementite Lamellae in a Cold-Drawn Pearlitic Wire

Tuo Xin[1] · Guiju Liu[1] · Wenshuang Liang[1] · Rongsheng Cai[1] · Honglei Feng[1] · Chen Li[1] · Jian Li[2] · Yiqian Wang[1]

Received: 13 November 2017 / Accepted: 25 January 2018 / Published online: 14 March 2018

Abstract
High-resolution transmission electron microscopy is used to investigate the deformation behaviors of cementite lamellae in the heavily cold-drawn piano wires. Three distinct morphologies of cementite are observed, namely, complete lamella, partly-broken lamella and nearly-disappeared lamella. For the complete cementite lamella, it remains a single-crystalline structure. For the partly-broken cementite lamella, polycrystalline structure and neck-down region appear to release the residual strain. The lattice expansion of ferrite takes place in two perpendicular directions indicating that the carbon atoms dissolve from cementite into ferrite lattices. An orientation relationship is found between ferrite and cementite phases in the cold-drawn pearlitic wire.

Keywords High-resolution transmission electron microscopy · Microstructure · Deformation · Cementite dissolution · Orientation relationship

1 Introduction

Heavily cold-drawn eutectoid pearlitic wires have been widely used in engineering such as springs, tyres and suspension bridge cables [1–4] because of their extremely high tensile strength (the maximum is up to 7 GPa [5]). It has been demonstrated that pearlite has a well-defined lamellar structure with cementite and ferrite phases alternately arranged after a cold-drawing process [6–8]. Substantially, ferrite in pearlite, the matrix phase, has excellent plasticity, and cementite in pearlite, the strengthening phase known as a brittle phase, is critical for the strengthening of the cold-drawn wires. The performance of pearlitic wires is closely related to the microstructure of two components, such as phase morphology (lamellae or particle), distribution (alternative-layer distribution or grain boundary distribution), size (lamellar spacing, particle size) and so on. A number of orientation relationships are found between the ferrite and cementite lamellae before drawing, while only three, namely, Bagaryatsky [9], Isaichev [10] and Pitsch–Petch [11] orientation relationships, are consistently reported in the literature. However, few investigations focus on the orientation relationship between ferrite and cementite after drawing. Thus, it is important to clarify the orientation relationship between ferrite and cementite in the cold-drawn pearlite.

More recently, the plastic deformation and dissolution of cementite in the cold-drawn pearlitic wires have received considerable attention. During the cold-drawing process, the ultrafine cementite lamellae display remarkable plasticity, in which some slip systems are proposed [12–14]. The pearlite lamellae are mainly subjected to tensile stress parallel to the drawing direction and the compressive stress normal to the drawing direction [15]. The lamellar spacing of cementite decreases progressively and the lamellar direction is gradually re-aligned along the drawing direction. Based on the Hall–Petch relationship, the strength of the cold-drawn wire is related with the lamellar spacing [2].

Tuo Xin and Guiju Liu have contributed equally to this work.

Electronic supplementary material The online version of this article (https://doi.org/10.1007/s12540-018-0101-z) contains supplementary material, which is available to authorized users.

✉ Yiqian Wang
yqwang@qdu.edu.cn

[1] College of Physics and The Cultivation Base for State Key Laboratory, Qingdao University, No. 308, Ningxia Road, Qingdao 266071, People's Republic of China

[2] School of Materials Science and Engineering, Zhejiang University, No. 38, Zheda Road, Hangzhou 310027, People's Republic of China

It has been confirmed that the cementite phase undergoes a dissolution process in which carbon atoms dissolve into the ferrite phase [7, 16–19]. When the drawing strain is less than a critical value, the solubility of carbon atom increases with the drawing strain, and it is no longer affected by the drawing strain when it reaches the critical value [7]. However, no special effort has been devoted to investigate the dissolution of cementite in a heavily cold-drawn state. A comprehensive understanding is still lacking for the plastic deformation and dissolution of cementite phase.

In this paper, the microstructure evolution of pearlite lamellae in heavily cold-drawn piano wires is investigated using transmission electron microscopy (TEM). Based on the microstructure analysis of cementite after the cold drawing, the dissolution mechanism of cementite is revealed. In addition, one new orientation relationship is found between cementite and ferrite phases.

2 Experimental

The piano wire in this study was produced according to Japanese Standard JIS G 3522. Its chemical composition is Fe–0.83C–0.45Mn–0.22Si–0.15Cu–0.02P–0.02S (wt%). The initial rod diameter is 4 mm, and the final diameter is reduced to 1.2 mm after the cold-drawing process. The total section area reduction is 91%. The strain ε of a cold-drawn wire is expressed using the following equation [2],

$$\varepsilon = 2\ln\left(D_0/D\right) \quad (1)$$

where D_0 and D refer to the diameter of the initial wire and the cold-drawn wire, respectively. The strain ε is calculated to be 2.4 in this study.

The microstructure of the piano wire was characterized by TEM. The specimens were prepared in a longitudinal sectional direction using conventional techniques of mechanical polishing and ion thinning. The ion milling was performed using a Gatan Model 691 precision ion polishing system (PIPS, Pleasanton, CA) at a low voltage, equipped with a cooling stage. The bright field (BF) imaging, selected-area electron diffraction (SAED) and high-resolution TEM (HRTEM) examinations were carried out using a JEOL JEM 2100F TEM operating at 200 kV. Before obtaining the HRTEM images for the piano wire, we carried out the calibration of TEM magnification using HRTEM images of single-crystalline gold film. The calibration procedure can be found in the Supplementary Information.

3 Results and Discussion

Figure 1a shows a typical BF TEM image of the specimen obtained at a low magnification. The pearlite lamellae (labeled by white arrows) are re-aligned along the drawing direction and keep a fine fibrous structure. To explore the detailed microstructure of the ferrite and cementite in pearlite, a high-magnification BF TEM image is shown in Fig. 1b. It can be clearly seen that wide and thin lamellae are alternately arranged, which correspond to ferrite labeled by F1, F2, … F11 and cementite indicated by white arrows, respectively. In addition, the interface between cementite and ferrite is obvious. The ferrite lamellae in the upper-right region are darker than those in the lower-left region, which is caused by diffraction contrast. Both cementite and ferrite lamellae become re-aligned nearly parallel to the drawing direction and consistently hold alternate fibrous structure with a few breakages. The average widths of ferrite and cementite lamellae are 135 and 14 nm, respectively. The width ratio of ferrite and cementite lamellae is about 9.6:1, which is larger than that before the drawing (9:1) [14]. It is indicated that both cementite and ferrite phases in the piano wire show excellent plastic deformation performance. In addition, it can be found that the cementite stripes among F4 and F11 in Fig. 1b are completely preserved and regularly arranged. However, the stripe between F3 and F4 is not continuous and breaks in some areas, suggesting that the

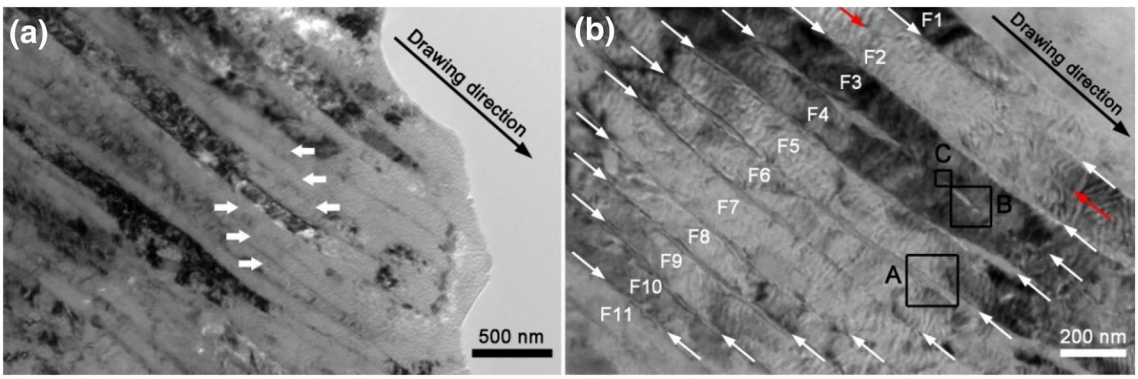

Fig. 1 Typical BF TEM images of the cold-drawn piano wire at a low magnification (**a**) and at a high magnification (**b**)

strain leads to the fragmentation of some cementite lamellae during the cold-drawing process. Moreover, the cementite stripes on F2 boundaries are partly broken and partly narrow down to a line. To clearly show the boundary, two red arrows label the trace of a cementite stripe in F2, which has nearly disappeared. Hence, it is reasonable to classify the cementite lamellae into three different morphologies after the heavy cold-drawing, complete lamellae, partly-broken lamellae and nearly-disappeared lamellae.

To clarify the microstructure of cementite in the heavily cold-drawn piano wire, extensive HRTEM examinations were carried out. Figure 2a displays a $[\bar{1}\bar{1}3]$ zone-axis HRTEM image of a complete cementite lamella taken from region A in Fig. 1b. The cementite lamella (labeled by Cem) is located between two ferrite lamellae (labeled by F5 and F6), separated by two dashed lines. The cementite lamella maintains its initial profile along the drawing direction, and the average width of this cementite lamella is measured to be 26.5 ± 0.1 nm, which is larger than usual width (10 nm) of cementite. This could result from the uneven distribution of drawing strain in the piano wire. In Fig. 2a, the atomic sequences of ferrite are unclear because it does not strictly conform to the Bragg diffraction condition. Both cementite and ferrite phases, although partially narrowing-down, hold complete continuity at the interface in the cold-drawing process. Figure 2b shows a typical SAED pattern taken from the interface region between cementite and ferrite. The diffraction spots are not circular but elongated, indicating that they belong to two phases, which can be indexed to $[\bar{1}\bar{1}3]$ zone-axis of cementite and $[\bar{1}11]$ zone-axis of ferrite. The sharp diffraction spots demonstrate that both cementite and ferrite lamellae remain single-crystalline structures after the cold-drawing process. From the above analysis, it is concluded that the wide cementite lamellae have excellent plasticity and still hold a complete structure during the cold-drawing process.

Figure 3a, b show HRTEM images of the partly-broken cementite lamellar structures between F3 and F4. Figure 3a shows a [001] zone-axis HRTEM image of ferrite in region B of Fig. 1b, where a partly-broken cementite lamella can be clearly seen between two ferrite lamellae. The average width of the cementite lamella is 15.2 ± 0.2 nm, which is thinner than that in Fig. 2a. The polycrystalline structures appear in the cementite lamella, which are labeled by Polyc Cem. Some regions are observed without crystal lattices,

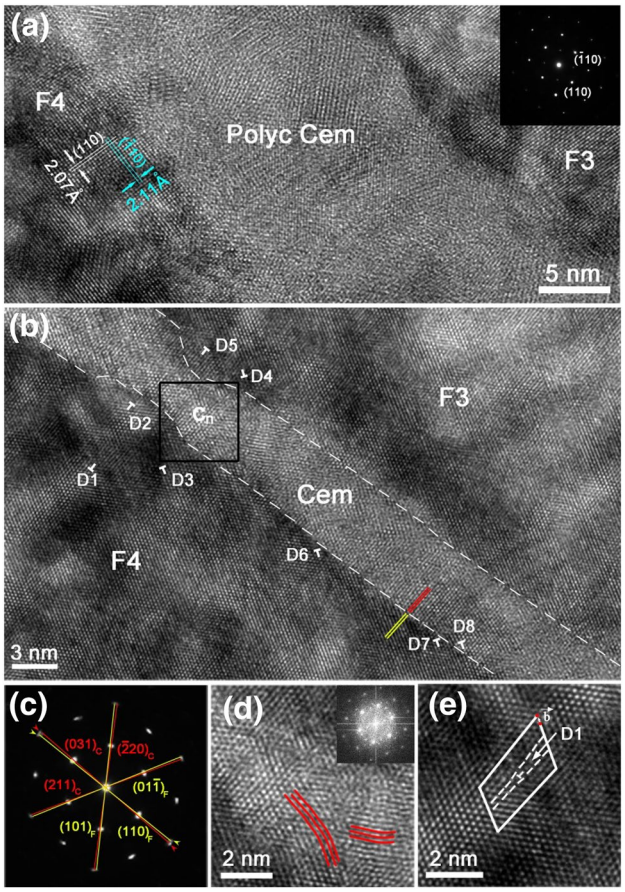

Fig. 3 **a**, **b** Typical HRTEM images of regions B and C in Fig. 1b, respectively, showing a partly-broken cementite lamella between F3 and F4. Inset is typical SAED pattern taken from ferrite area, **c** the corresponding SAED pattern taken from the interface region between cementite and ferrite in (**b**), **d** typical HRTEM image and the FFT pattern of the neck-down part of cementite in region "c_n", **e** Burgers circuit for dislocations D1

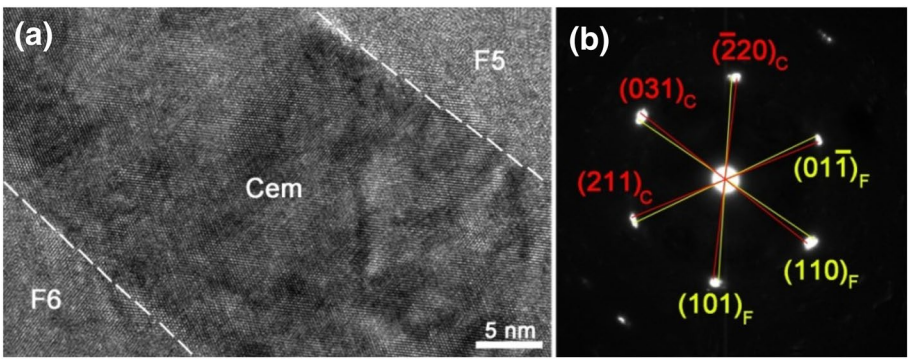

Fig. 2 **a** Typical HRTEM image taken from region A in Fig. 1b, showing a complete cementite lamella between F5 and F6, **b** the corresponding SAED pattern taken from the interface region between cementite and ferrite

which might be due to differently-oriented grains in the TEM sample. This HRTEM image indicates that the original single-crystalline structure of cementite is destroyed by the large strain in the cementite lamella. In Fig. 3a, {110} planes of ferrite are marked by two pairs of parallel lines. The angle between these two pairs of parallel lines is 90°. Inset of Fig. 3a shows a typical [001] zone-axis SAED pattern taken from the ferrite area. Through measuring more than 10 lattice fringes of ferrite, the average interplanar spacings for $(\bar{1}10)_F$ and $(110)_F$ are determined to be 2.11 and 2.07 Å, respectively, both of which are larger than the theoretical value (d_{110} = 2.02 Å). This means that the interplanar spacings of the ferrite phase are dilated, both normal to and parallel to the drawing direction.

Figure 3b shows a $[\bar{1}11]$ zone-axis HRTEM image of ferrite in region C of Fig. 1b, showing another partly-broken cementite lamella. In Fig. 3b, the interface between cementite and ferrite lamellae is labeled by dashed lines. It is interesting to observe a neck-down region in the cementite lamella at an atomic scale, which has never been reported before. The average width of this cementite lamella is measured to be 5.5 ± 0.2 nm, and the smallest width of 2.4 ± 0.1 nm is observed in the neck-down region of this cementite lamella. The decreasing lamellar width indicates that this cementite lamella undergoes severe deformation during the cold-drawing process. Dislocations gradually appear near the interface region, contributing to the plastic deformation of cementite and ferrite lamellae. Several dislocations are labeled by D1–D8. In addition, the lattice fringes (labeled by two yellow lines) of ferrite are parallel to those (labeled by two red lines) of cementite, demonstrating that the interface between cementite and ferrite lamellae is continuous. Figure 3c is the SAED pattern taken from the boundary region of ferrite and cementite phases. It shows two sets of diffraction spots, one set being indexed to ferrite phase, the other being indexed to cementite phase. Figure 3d shows an enlarged HRTEM image of the neck-down region [rectangular region "c_n" in Fig. 3b]. Inset shows the fast Fourier transform (FFT) pattern of this region, which can be indexed as $[\bar{1}\bar{1}3]$ zone-axis of cementite. Careful examination of HRTEM image shows that the atomic plane bending (labeled by red lines) of cementite takes place in some regions. The observed lattice bending could be caused by either the projection effect or the large load force during the cold-drawing process. More dislocations are found to form near the neck-down region than the other regions. To identify the extra half atomic planes more clearly, Fig. 3e shows an enlarged HRTEM image of one edge dislocations D1. It is clearly seen that there is a gap between the starting and ending point in the Burgers circuit, as indicated by an arrow. The Burgers vector for dislocation D1 is determined to be 1/2 <211>, which is a characteristic vector for a perfect dislocation in the ferrite lattice.

In general, during the cold-drawing process, to remain constant volume of the unit cell, the interplanar spacing of the planes parallel to the drawing direction should decrease, while the interplanar spacing of the planes normal to the drawing direction should increase. However, in our HRTEM observation (Fig. 3a), the lattice spacings for the two perpendicular planes are all dilated. Moreover, the lattice spacing of the planes parallel to the drawing direction is larger than that of the planes perpendicular to the drawing direction. This is attributed to the synergistic effect between the tensile strain and dissolution of the cementite lamella during the cold-drawing process. From a macroscopic view, the lamellae are subjected to a tensile stress parallel to the drawing direction and a compressive stress normal to the drawing direction, leading to a lengthwise direction deformation and a reduction of wire diameter. However, from a microscopic view, the plastic deformation process within the wire lattice is a shear process, in which the direction of shear-slip atomic plane is not consistent with that of tensile load. With the accumulation of shear strain, the carbon atoms released from the cementite dissolve into the ferrite lattice. According to the martensitic transformation theory [20], the carbon atoms can occupy the sites of three bcc sublattices of octahedral interstitial positions. Therefore, the carbon atoms are not evenly distributed in the octahedral interstices of ferrite during the shear process of phase transformation, which dilates the spacings of different ferrite planes with various increment. This might lead to the fact that the lattice spacing of the ferrite planes parallel to the drawing direction is larger than that of the planes perpendicular to the drawing direction. When some dislocations form on both sides of cementite lamella, the isolated carbon atoms are easily trapped by the dislocations during the cold-drawing process [21–23], and they can glide through the dislocations near the interface into the ferrite lattice, resulting in the dissolution of cementite and the lattice expansion of ferrite. The more dislocations, the more cementite will be dissolved, which could lead to the formation of neck-down regions as shown in Fig. 3b.

Through careful examination of the SAED patterns in Figs. 2b and 3c, we find that cementite and ferrite phases possess an orientation relationship after the cold-drawing process, which is determined to be $[\bar{1}\bar{1}3]_C//[\bar{1}11]_F$, $(031)_C$ 2.5° from $(\bar{1}\bar{1}0)_F$, $(\bar{2}20)_C//(\bar{1}0\bar{1})_F$ and $(211)_C//(0\bar{1}1)_F$. The orientation relationship between cementite and ferrite phases in the cold-drawn pearlites is rarely reported, although some can be found for the cold-rolled pearlites. This finding is significant because it provides direct evidence for the orientation relationship between ferrite and cementite in the cold-drawn pearlite.

Figure 4 shows a typical HRTEM image of a nearly-disappeared cementite lamellar structure (labeled by two red arrows) between F1 and F2 in Fig. 1b. It is clearly seen that

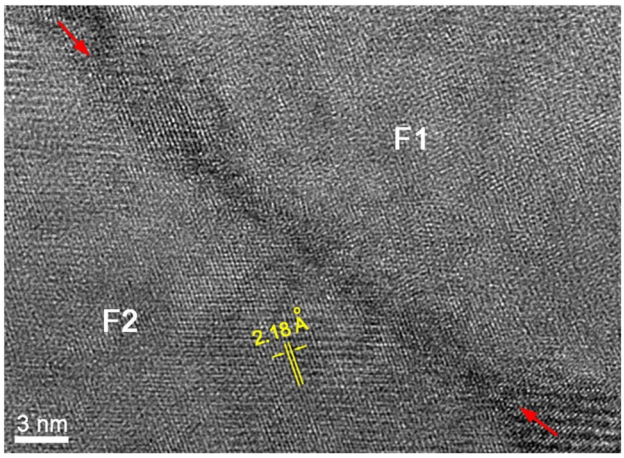

Fig. 4 Typical HRTEM image of the nearly-disappeared cementite lamellar structure between F1 and F2

the cementite stripe has a dumbbell-like profile and the middle part of cementite lamella is quite narrow and nearly disappears, where a retained trace of the cementite phase can be found. It suggests that the initial cementite lamella is nearly dissolved under the large drawing strain. In F2 lamella, the lattice spacing is measured to be 2.18 Å, which is larger than the theoretical value of {110} planes of ferrite, indicating that the crystal lattices of ferrite undergo a severe expansion. In addition, the lattice spacing is larger than that in Fig. 3a, indicating that more carbon atoms dissolve into the ferrite lattice in Fig. 4, which leads to the nearly-disappeared cementite lamellar structure.

4 Conclusions

The deformation behaviors of cementite lamellae in the cold-drawn piano wire have been investigated using HRTEM. Three distinct morphologies of cementite are observed, namely, complete lamella, partly-broken lamella and nearly-disappeared lamella. For the complete cementite lamella, it remains a single-crystalline structure. For the partly-broken cementite lamella, polycrystalline structure and neck-down regions appear to release the residual strain. The dissolution of cementite results in the lattice expansion of ferrite phase and the appearance of neck-down regions in the cementite phase. The cementite and ferrite phases possess an orientation relationship after the cold-drawing process.

Acknowledgements We would like to thank the financial support from the National Natural Science Foundation of China (Grant No. 10974105) and High-end Foreign Experts Recruitment Programs (Grant Nos. GDW20173500154, GDW20163500110). Y. Q. Wang would also like to thank the financial support from the Top-notch Innovative Talent Program of Qingdao City (Grant No. 13-CX-08), Taishan Scholar Program of Shandong Province, Qingdao International Center for Semiconductor Photoelectric Nanomaterials and Shandong Provincial University Key Laboratory of Optoelectrical Material Physics and Devices.

References

1. D. Raabe, P. Choi, Y.J. Li, A. Kostka, X. Sauvage, F. Lecouturier, K. Hono, R. Kirchheim, R. Pippan, D. Embury, MRS Bull. **35**, 982 (2010)
2. X.D. Zhang, A. Godfrey, X.X. Huang, N. Hansen, Q. Liu, Acta Mater. **59**, 3422 (2011)
3. K. Hono, M. Ohnuma, M. Murayama, S. Nishida, A. Yoshie, T. Takahashi, Scr. Mater. **44**, 977 (2001)
4. W. Lojkowski, M. Djahanbakhsh, G. Bürkle, S. Gierlotka, W. Zielinski, H.-J. Fecht, Mater. Sci. Eng. A **303**, 197 (2001)
5. Y.J. Li, D. Raabe, M. Hernig, P.P. Choi, S. Goto, A. Kostka, H. Yarita, C. Borchers, R. Kirchheim, Phys. Rev. Lett. **113**, 106104 (2014)
6. J. Languillaume, G. Kapelski, B. Baudelet, Mater. Lett. **33**, 241 (1997)
7. W.J. Nam, C.M. Bae, S.J. Oh, S.J. Kwon, Scr. Mater. **42**, 457 (2000)
8. H.G. Read, W.T. Reynolds Jr., K. Hono, T. Tarui, Scr. Mater. **37**, 1221 (1997)
9. D.S. Zhou, G.J. Shiflet, Metall. Mater. Trans. A **23**, 1259 (1992)
10. Y. Adachi, S. Morooka, K. Nakajima, Y. Sugimoto, Acta Mater. **56**, 5995 (2008)
11. M.-X. Zhang, P. Kelly, Scr. Mater. **37**, 2009 (1997)
12. F. Fang, Y.F. Zhao, P.P. Liu, L.C. Zhou, X.J. Hu, X.F. Zhou, Z.H. Xie, Mater. Sci. Eng. A **608**, 11 (2014)
13. Y. Ivanisenko, W. Lojkowski, R.Z. Valiev, H.-J. Fecht, Acta Mater. **51**, 5555 (2003)
14. J. Languillaume, G. Kapelski, B. Baudelet, Acta Mater. **45**, 1201 (1997)
15. J. Toribio, Mater. Sci. Eng. A **387–389**, 227 (2004)
16. C.W. Bang, J.B. Seol, Y.S. Yang, C.G. Park, Scr. Mater. **108**, 151 (2015)
17. C. Borchers, T. Al-Kassab, S. Goto, R. Kirchheim, Mater. Sci. Eng. A **502**, 131 (2009)
18. X. Sauvage, W. Lefebvre, C. Genevois, S. Ohsaki, K. Hono, Scr. Mater. **60**, 1056 (2009)
19. Y. Todaka, M. Umemoto, A. Ohno, M. Suzuki, Y. Kawabata, K. Tsuchiya, J. Alloys Compd. **434–435**, 497 (2007)
20. C. Zener, Kinetics of the decomposition of austenite. Trans. AIME **167**, 550 (1946)
21. V.N. Gridnev, V.V. Nemoshkalenko, Y.Y. Meshkov, V.G. Gavriliyuk, V.G. Prokopenko, O.N. Raumov, Phys. Status Solidi A **31**, 201 (1975)
22. V.G. Gavriljuk, Mater. Sci. Eng. A **345**, 81 (2003)
23. X. Sauvage, J. Copreaux, F. Danoix, D. Blavette, Philos. Mag. A **80**, 781 (2000)